Int J Thermophys (2010) 31:1273–1293
DOI 10.1007/s10765-010-0754-4

Cylindrical Acoustic Resonator for the Re-determination of the Boltzmann Constant

J. T. Zhang · H. Lin · J. P. Sun · X. J. Feng · K. A. Gillis · M. R. Moldover

Received: 21 October 2009 / Accepted: 10 May 2010 / Published online: 1 June 2010

Abstract The progress towards re-determining the Boltzmann constant k_B using two fixed-path, gas-filled, cylindrical, acoustic cavity resonators is described. The difference in the lengths of the cavities is measured using optical interferometry. Thus, a literature value for the density of mercury is not used, in contrast with the presently accepted determination of k_B. The longitudinal acoustic resonance modes of a cylindrical cavity have lower quality factors Q than the radial modes of gas-filled, spherical cavities, of equal volume. The lower Qs result in lower signal-to-noise ratios and wider, asymmetric resonances. To improve signal-to-noise ratios, conventional capacitance microphones were replaced with 6.3 mm diameter piezoelectric transducers (PZTs) installed on the outer surfaces of each resonator and coupled to the cavity by diaphragms. This arrangement preserved the shape of the cylindrical cavity, prevented contamination of the gas inside the cavity, and enabled us to measure the longitudinal resonance frequencies with a relative standard uncertainty of 0.2×10^{-6}. The lengths of the cavities and the modes studied will be chosen to reduce the acoustic perturbations due to non-zero boundary admittances at the endplates, e.g., from endplate bending and ducts and/or transducers installed in the endplates. Alternatively, the acoustic perturbations generated by the viscous and thermal boundary layers at the gas–solid boundary can be reduced. Using the techniques outlined here, k_B can be re-determined with an estimated relative standard uncertainty of 1.5×10^{-6}.

J. T. Zhang (✉) · H. Lin · J. P. Sun
National Institute of Metrology, 100013 Beijing, China
e-mail: zhangjint@nim.ac.cn

X. J. Feng
Tsinghua University, 100084 Beijing, China

K. A. Gillis · M. R. Moldover
National Institute of Standards and Technology, Gaithersburg, MD 20899-8360, USA

Keywords Boltzmann constant · Cylindrical acoustic resonator · Two-color interferometry

1 Introduction

The acoustic resonance method is a means for accurate measurements of the speed of sound in dilute gases. Accurate speed-of-sound data have been used to determine the thermophysical properties of fluids [1–5], thermodynamic temperatures [6–10], and the universal gas constant [11,12]. The acoustic resonance method is one of the most accurate methods now being used by several laboratories to re-determine the Boltzmann constant in preparation for the new definition of the kelvin [13]. The accurate measurement of acoustic resonance frequencies in dilute gases requires non-degenerate resonance modes. These modes include the radially symmetric modes of a spherical or cylindrical cavity and the longitudinal modes of a cylindrical cavity. Under typical conditions (argon, 273 K, 100 kPa, 50 mm radius), the first five radially symmetric, gas resonance modes of an argon-filled spherical cavity have quality factors Q in the range from 2000 to 3700. Because the Qs are high, the modes are well separated from nearby degenerate modes and they have high signal-to-noise ratios. Under the same conditions, the first five non-degenerate longitudinal gas resonance modes of a cylinder (radius $a = 50\,\text{mm}$, length $L = 100\,\text{mm}$) have Qs that are approximately 1/5th as large. (Much of the reduction of the Qs originates in the viscous damping of the longitudinal acoustic modes of a cylindrical cavity.) Therefore, it is more difficult to measure the frequencies of the longitudinal acoustic modes of a cylinder with the same accuracy as the radial modes of sphere. This difficulty is partially offset by the simplicity of machining a cylindrical cavity and the simplicity of measuring its length.

We describe progress towards re-determining the Boltzmann constant k_B using two fixed-path, gas-filled, cylindrical, acoustic cavity resonators. This work builds upon the pioneering measurements of Quinn et al. [14] and Colclough et al. [11] who used a cylindrical cavity to re-determine the universal gas constant R (and also the Boltzmann constant because the value of the Avogadro constant $N_\text{A} = R/k_\text{B}$ was well known). These authors changed the length of their cavity by 140 mm by moving a piston within a cylinder. They used an optical interferometer to measure the length changes, and they measured the amplitude and phase of the sound pressure at one end of the cavity, while the cavity was excited at the constant frequency of 5.6 kHz. Thus, their data determined the wavelength of sound at 5.6 kHz. They used a slender cylinder ($a = 15\,\text{mm}$) so that only longitudinal modes would propagate at the operating frequency. However, the fixed end of their cylinder was the diaphragm of a loud speaker that both generated and detected sound. The diaphragm was a 0.25 mm thick aluminum alloy film which had a non-zero acoustic admittance. Unfortunately, this admittance led to a non-linear speaker response as a function of the gas pressure that was discovered only after the initial publication of a re-determination of the gas constant [11,14]. The variable-length resonator had additional complications. The movable assembly was troublesome to align. The acoustic admittance of the gap between the piston and the cylinder interior was hard to characterize. A very narrow gap would have caused excessive friction, and a wide gap would have a large admittance that would generate

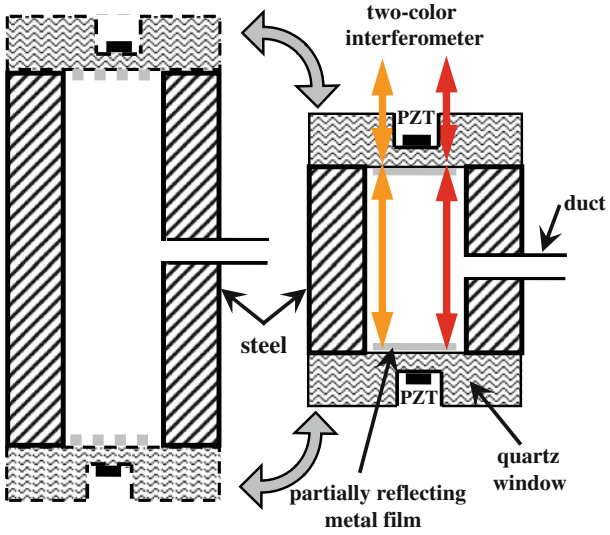

Fig. 1 Schematic diagram of two fixed-length, cylindrical, cavity resonators with interchangeable ends

large-frequency and pressure-dependent perturbations to the acoustic field within the cavity that would add to the uncertainty of the results.

The key features of our apparatus are displayed in Fig. 1. In contrast with Colclough et al. and Quinn et al. [11,14], we use two, fixed-length, cylindrical cavities because they are easy to manufacture and assemble. Because a fixed-length cavity does not have a sliding seal, we can isolate the gas inside the cavity from the gas in the surrounding pressure vessel to avoid contaminating the gas. The thick endplates have a small mechanical admittance, and a PZT transducer is installed in a blind hole in each endplate. This transducer scheme avoids the problem of the non-linear response of a loud speaker and it generates larger signals than the small capacitive microphones that are often used in metrological applications of gas-filled acoustic resonators. We use the same endplates for both the cylinders, and we deduce the speed of sound from the difference between the lengths of the two cavities. This length difference is determined by two-color optical interferometry. The measured length difference is insensitive to the optical phase shifts in the thin-film metallic mirrors. If an absolute length determination were required, these phase shifts would have to be determined. As discussed below, we choose the lengths of the cavities and the modes studied to achieve specific experimental objectives such as reducing the uncertainties from either the hard-to-estimate acoustic perturbations from the bending of the endplates of the cylinders or the comparatively large, but well-understood, frequency perturbations that result from the thermal and viscous boundary layers.

In this study, we consider three challenges: (1) the perturbations from the cavities' boundaries, (2) the determination of the resonance frequencies, and (3) the measurement of the lengths of the cavities. Using the techniques outlined here, we estimate that k_B can be re-determined with a relative standard uncertainty $u_r(k_B) = 1.5 \times 10^{-6}$.

2 Normal Modes of a Cylindrical Cavity

We assume that the gas inside a cylindrical cavity of length L and the radius a is driven by a steady, sinusoidal source. We assume that the amplitude of the acoustic oscillations is small enough that non-linearity can be neglected [15,16]. As a first approximation, we assume the shell surrounding the cavity is perfectly rigid and does not conduct heat and we ignore the viscous damping of the gas in contact with the shell. With these approximations, the admittance of the gas–shell interface is zero. The normal modes of the gas are acoustic pressure waves with spatial dependence:

$$\varphi_{lmn}(r,\theta,z) = J_m\left(\frac{\chi_{mn} r}{a}\right)[\cos(m\theta)+\sin(m\theta)]\cos\left(\frac{l\pi z}{L}\right), \tag{1}$$

where the origin of the cylindrical coordinate system is located on the symmetry axis at one end of the cavity. Here, l, m, and n are integers; J_m is the mth-order Bessel function of the first kind; and χ_{mn} is a root of the equation $\mathrm{d}J_m(\chi)/\mathrm{d}\chi = 0$. We use the triplet of integers (l, m, n) to refer to a specific mode, where $l = 0, 1, 2, \ldots$ is the longitudinal index, $m = 0, \pm1, \pm2, \ldots$ is the azimuthal index, and $n = 0, 1, 2, \ldots$ is the radial index.[1] The resonance frequency of the (l, m, n) mode is

$$f^0_{lmn} = \frac{c}{2\pi}\sqrt{\left(\frac{l\pi}{L}\right)^2 + \left(\frac{\chi_{mn}}{a}\right)^2}, \tag{2}$$

where c is the speed of sound in the gas, and the superscript "0" of f^0_{lmn} refers to the idealized (or "unperturbed") boundary conditions. Due to the symmetry of the Bessel function $J_{-m}(x) = (-1)^m J_m(x)$, the modes for which $m \neq 0$ are doubly degenerate, i.e., the resonance frequencies of the modes (l, m, n) and $(l, -m, n)$ are exactly the same. For the non-degenerate, longitudinal gas modes denoted $(l, 0, 0)$, $\chi_{mn} = 0$ and the ideal unperturbed frequencies are determined only by the length of the cylinder and the speed of sound in the gas:

$$f^0_{l00} = \frac{cl}{2L}. \tag{3}$$

3 Frequency Perturbations

Table 1 lists the unperturbed frequencies of several longitudinal modes $(l, 0, 0)$ of argon at 273.16 K and 100 kPa in three cylinders with lengths of 80.7 mm, 129.1 mm, and 161.4 mm. (Each cylinder has an 80 mm inside diameter and 25 mm thick steel walls.) Table 1 also lists estimated perturbations of these modes from the viscous, thermal, and mechanical admittances of the walls of the cavity and from a fill duct

[1] The notation that we use was adopted from Ref. [15], Sect. 9.2, which describes the modes of circular ducts. The mode designated (l, m, n) has l nodal planes perpendicular to the cylindrical axis, $|m|$ nodal planes extending radially outward from the axis, and n cylindrical nodal surfaces concentric with the axis. Our notation differs from that of Ref. [16], for which the third number in the triplet $n' = n + 1$.

Table 1 Calculated unperturbed frequencies and fractional frequency perturbations of several longitudinal acoustic modes of argon-filled cavities of radius $a = 40$ mm and length L

L (mm)	l	Unpert. freq.	Boundary layer		Shell motions				Transducers	Fill duct
		f^0 (Hz)	Thermal $\frac{\Delta f_T}{f^0} \times 10^6$	Viscous $\frac{\Delta f_v}{f^0} \times 10^6$	Radial stretch $\frac{\Delta f_{sh1}}{f^0} \times 10^6$	Axial stretch $\frac{\Delta f_{sh2}}{f^0} \times 10^6$	Bending of ends $\frac{\Delta f_{sh3}}{f^0} \times 10^6$	Free-body recoil $\frac{\Delta f_{sh4}}{f^0} \times 10^6$	$\frac{\Delta f_{tr}}{f^0} \times 10^6$	$\frac{\Delta f_d}{f^0} \times 10^6$
80.7	1	1907	−912.8	−557.9	−0.23	0	−10.5	−42.72	−0.27	0.00
	2	3815	−645.5	−394.5	−0.26	−1.00	−11.5	0	−0.27	−0.22
	3	5722	−527.0	−322.1	−0.10	0	−13.6	−4.75	−0.27	0.00
	4	7630	−456.4	−279.0	−0.04	−1.13	−18.2	0	−0.28	−0.07
129.1	4	4768	−469.8	−353.2	−0.16	−1.06	−7.7	0	−0.17	−0.09
	6	7152	−383.5	−288.4	−0.04	−1.23	−10.4	0	−0.17	−0.05
	8	9536	−332.1	−249.8	−0.01	−1.56	−20.3	0	−0.18	−0.03
	12	14304	−271.3	−204.0	−0.00	−7.44	11.9	0	−0.20	0.00
161.4	2	1907	−685.6	−557.9	−0.66	−0.98	−5.3	0	−0.13	−0.44
	4	3815	−484.8	−394.5	−0.29	−1.04	−5.8	0	−0.14	−0.14
	6	5722	−395.8	−322.1	−0.09	−1.16	−6.8	0	−0.14	−0.07
	8	7630	−342.8	−279.0	−0.03	−1.39	−9.1	0	−0.14	−0.04

The perturbations are calculated for argon at 273.16 K and 100 kPa and the results are multiplied by 10^6

and transducers. In Sect. 3.1, we describe the origin of the tabulated estimates, and in Sect. 3.2, we discuss ways of accounting for the perturbations.

3.1 Estimating Frequency Perturbations

3.1.1 Thermoacoustic Boundary Layer

The gas–shell boundary has non-zero thermal and viscous admittances that cause the measured resonance frequencies to differ from their unperturbed values. The longitudinal acoustic oscillations are subject to viscous damping in a boundary layer of gas in contact with the surrounding shell. The damping reduces the resonance frequency by $|\Delta f_{\mathrm{v}}|$ and increases the half-width of the resonance by g_{v}:

$$\frac{(g_{\mathrm{v}})_{l00}}{f^0} = -\frac{(\Delta f_{\mathrm{v}})_{l00}}{f^0} = \frac{\delta_{\mathrm{v}}}{2a} = \frac{1}{2a}\sqrt{\frac{2\eta}{\rho\omega}}. \tag{4}$$

Here, δ_{v} is the length that characterizes the penetration of the viscous boundary layer into the gas, η is the viscosity, ρ is the density, and $\omega \equiv 2\pi f$ is the angular frequency of the acoustic oscillation [3].

The irreversible heat exchange between the gas oscillating in the cavity and the shell surrounding the cavity reduces the resonance frequency by $|\Delta f_{\mathrm{T}}|$ and increases the half-width of the resonance by g_{T}:

$$\frac{(g_{\mathrm{T}})_{l00}}{f^0_{lmn}} = -\frac{(\Delta f_{\mathrm{T}})_{l00}}{f^0_{lmn}} = (\gamma-1)\frac{\delta_{\mathrm{T}}}{2a}\left(1+\frac{2a}{L}\right) = \frac{(\gamma-1)}{2a}\sqrt{\frac{2D_{\mathrm{T}}}{\omega}}\left(1+\frac{2a}{L}\right). \tag{5}$$

Here, δ_{T} is the length that characterizes the penetration of the thermal boundary layer from the cavity's wall into the gas, $D_{\mathrm{T}} \equiv \lambda/(\rho C_p)$ is the thermal diffusivity, λ is the thermal conductivity, C_p and C_v are the constant-pressure and constant-volume specific heats, and $\gamma \equiv C_p/C_v$ is the adiabatic index [3].

3.1.2 Mechanical Admittance of the Shell

The shell surrounding the cavity deforms in response to the acoustic pressure in the gas. In general, the mechanical admittance associated with these deformations (and the corresponding frequency perturbations and contributions to the half-widths) is difficult to calculate. We calculate four simple, model deformations that have been considered in the literature: (1) uniform radial (Δf_{sh1}) and (2) uniform axial (Δf_{sh2}) deformations of an infinite cylinder, and (3) bending of the endplates (Δf_{sh3}), and (4) longitudinal recoil (Δf_{sh4}) of the shell treated as a rigid body. The shell does not recoil when the spatial average of the momentum of the gas is zero; therefore, Δf_{sh4} is zero for the $(l, 0, 0)$ modes when l is an even integer. The perturbations due to the model deformations are listed in Table 1.

To estimate the perturbation from axially symmetric radial deformation, we use a model for acoustic waves in a long pipe with flexible walls [17]. The compliance of the side wall lowers the resonance frequency just as it lowers the phase velocity of an acoustic wave propagating through a gas in a pipe [15]. To account for the resonator's finite length in the model, we use periodic simply supported boundary conditions with period L and apply the spatially varying pressure of the lth longitudinal gas mode. The mode's resonance frequency is shifted by the fractional amount,

$$\frac{\Delta f_{\mathrm{sh1}}}{f^0_{l00}} \approx -\frac{(\rho c^2)_{\mathrm{g}}}{\left(\rho_{\mathrm{ss}} c^2_{\mathrm{p,ss}}\right)} \left(\frac{a}{h}\right) \sum_{q=1}^{\infty} (B_{lq})^2 \frac{(k_{\mathrm{ss,q}} a)^2 - \Omega_l^2}{\left(\Omega^2_{\mathrm{w,q}} - \Omega_l^2\right)\left(\Omega^2_{\mathrm{u,q}} - \Omega_l^2\right)} \tag{6}$$

where $\Omega_l \equiv 2\pi f^0_{l00} a / c_{\mathrm{p,ss}}$, $k_q a = q\pi a / L$, h is the thickness of the shell, and the subscripts "g" and "ss" refer to properties of the gas and stainless-steel, respectively. The dimensionless parameters $\Omega_{\mathrm{w,q}}$ and $\Omega_{\mathrm{u,q}}$ are related to the radial and axial resonance frequencies of the shell, respectively:

$$f_{\mathrm{w,q}} = \frac{c_{\mathrm{p,ss}} \Omega_{\mathrm{w,q}}}{2\pi a} = \frac{c_{\mathrm{p,ss}}}{2\sqrt{2}\pi a} \Gamma_q^+ \quad \text{and} \quad f_{\mathrm{u,q}} = \frac{c_{\mathrm{p,ss}} \Omega_{\mathrm{u,q}}}{2\pi a} = \frac{c_{\mathrm{p,ss}}}{2\sqrt{2}\pi a} \Gamma_q^-$$
$$\text{with} \quad \left(\Gamma_q^{\pm}\right)^2 = 1 + k_q^2 a^2 + \beta^2 k_q^4 a^4 \pm \sqrt{\left(1 - k_q^2 a^2 + \beta^2 k_q^4 a^4\right)^2 + 4\nu^2 k_q^2 a^2} \tag{7}$$

where $c^2_{\mathrm{p,ss}} \equiv Y/[\rho_{\mathrm{ss}}(1-\nu^2)]$ is the speed of sound in a plate, Y is Young's modulus, ν is Poisson's ratio, and $\beta = h/(a\sqrt{12})$. For the 80.7 mm long resonator, $f_{\mathrm{w,1}} \approx 33$ kHz and $f_{\mathrm{u,1}} \approx 21$ kHz. The coefficient $B_{lq} = (2q/\pi)\left[1 + (-1)^{1+l+q}\right]/\left(q^2 - l^2\right)$ for $q \neq l$ and $B_{ll} = 0$. Only the first three or four non-zero terms in Eq. 6 were necessary to achieve convergence.

The axial stress on the cylindrical shell from the endplates causes an axial strain for the gas resonances modes with $l = \{\text{even integer}\}$. For the modes with $l = \{\text{odd integer}\}$ numbered gas modes, the unbalanced force causes recoil, which is handled separately. The perturbation from the axial stress was estimated from the expression,

$$\frac{\Delta f_{\mathrm{sh2}}}{f^0_l} \approx -\frac{(\rho c^2)_{\mathrm{g}}}{(\rho c^2)_{\mathrm{ss}}} \left(\frac{a}{\bar{a}}\right)\left(\frac{a}{h}\right) \frac{1}{1 - \left(f^0_l / f_{\mathrm{axial}}\right)^2} \tag{8}$$

for the even longitudinal modes, where $\bar{a}$ is the average radius of the shell, $f_{\mathrm{axial}} = 18.6$ kHz for $L = 80$ mm and 13.2 kHz for $L = 160$ mm. The resonance frequency f_{axial} was estimated from the axial stiffness of the cylindrical walls and the mass of the endplates. The contribution from odd longitudinal modes is zero to first order.

We considered two extreme models to estimate the perturbation from bending of the endplates. First, we assumed that they were simply supported around the circumference of a circle with radius $\bar{a}$. Under this assumption, we calculated the endplate perturbation from the expression,

$$\frac{\Delta f_{\mathrm{sh3}}}{f_l^0} \approx -\frac{1}{16}\frac{7+\nu}{1+\nu}\frac{\left(\rho c^2\right)_{\mathrm{g}}}{\left(\rho c_{\mathrm{p}}^2\right)_{\mathrm{FS}}}\left(\frac{2a}{L}\right)\left(\frac{\bar{a}}{a}\right)\left(\frac{\bar{a}}{h}\right)^3\frac{1}{1-\left(f_l^0/f_{\mathrm{bend}}\right)^2} \tag{9}$$

where $f_{\mathrm{bend}} = (0.217)hc_{\mathrm{p,FS}}/a^2 \approx 11.5\,\mathrm{kHz}$, and the subscript "FS" refers to fused silica. We listed these results in Table 1. Alternatively, we estimated the endplate perturbation using the assumption that the plates are clamped to a rigid cylinder around the circumference of the circle with radius $\bar{a}$. This assumption reduces the perturbation by approximately a factor of 10 and raises the resonance frequency. Because the endplates are bolted to the cylinder, the true boundary condition is probably between these extremes and might depend upon details such as the torque used to bolt the endplates to the cylinders.

Finally, the contribution from rigid-body recoil applies to the odd longitudinal modes. The correction is proportional to the ratio of the kinetic energies of the solid and the gas,

$$\frac{\Delta f_{\mathrm{sh4}}}{f} = \frac{1}{2}\frac{KE_{\mathrm{solid}}}{KE_{\mathrm{fluid}}} = \left(\frac{2}{l\pi}\right)^2\frac{M_{\mathrm{gas}}}{M_{\mathrm{res}}}, \quad \text{odd}\, l \tag{10}$$

where the last equality is in terms of the total mass of the gas M_{gas} and the mass of the resonator M_{res}. This correction is for a free body. In actuality, the resonators are supported by a complex structure that has resonances of its own. The response of the structure to vibrations of the resonator is very difficult to estimate or measure. Therefore, we recommend avoiding the asymmetric modes since they couple more strongly to the support structure than do the symmetric modes.

3.1.3 Transducers

The perturbation produced by a diaphragm in the endplate of a cylindrical cavity was modeled by Lin et al. [18]. Here, we use their result to estimate the perturbation from two fused-silica diaphragms that were located opposite each other at the ends of the cylindrical cavity. Each fused silica endplate had an integrated diaphragm to which a piezoceramic disk transducer was attached. The diaphragm had a diameter $2a_{\mathrm{dm}} = 10\,\mathrm{mm}$ and a thickness $t_{\mathrm{dm}} = 0.5\,\mathrm{mm}$ and was flush with the endplate's inner surface. The diaphragm was modeled as a thin plate that was clamped around its perimeter. The piezoceramic disk was made from lead zirconium titanate (PZT) and had a diameter of 6.4 mm and a thickness of 0.4 mm. The PZT disk was bonded to the outer surface of each diaphragm and it was concentric with the diaphragm. When the diaphragm deflected in response to the acoustic pressure in the cavity, the largest bending stress occurred in the fused-silica diaphragm near its perimeter. Therefore, the low-frequency compliance was determined from the properties of the diaphragm only. The diaphragm's flexure in response to the oscillating acoustic pressure modifies the surface admittance and shifts the gas's resonance frequency by an amount given by

$$\frac{\Delta f_{\rm tr}}{f_l^0} = -\frac{1}{16}\frac{\left(\rho c^2\right)_{\rm g}}{\left(\rho_{\rm FS} c_{\rm p,FS}^2\right)}\left(\frac{2a}{L}\right)\left(\frac{a_{\rm dm}}{a}\right)^3\left(\frac{a_{\rm dm}}{t_{\rm dm}}\right)^3\frac{1}{1-\left(f_l^0/f_{\rm dm}\right)^2} \tag{11}$$

The diaphragm's resonance frequency, $f_{\rm dm} \approx 38\,{\rm kHz}$, was calculated by modeling the diaphragm as a clamped plate loaded with the additional mass of a PZT transducer ($\sim$98 mg).

3.1.4 Fill Duct

As sketched in Fig. 1, a duct that admits gas into each cavity is attached to the side of each cylinder, midway between the ends of the cylinder. The perturbation produced by a cylindrical duct ($\Delta f_{\rm d}$ in Table 1) was modeled by Gillis et al. [19]. Here, we assumed the duct had an inner diameter of 1.4 mm and an infinite length. Note: for the $(l, 0, 0)$ modes when l is an even integer, there is a pressure node at the mid-plane of the resonator; therefore, $\Delta f_{\rm d} = 0$ for these modes, in the first order of the theory.

3.2 Accounting for the Larger Frequency Perturbations

The model for the cylindrical resonator predicts the measured resonance frequency f_N is related to the unperturbed (ideal) resonance frequency f^0 by

$$f^0 = f_N - \Delta f_{\rm b} - \Delta f_{\rm d} - \Delta f_{\rm sh} - \Delta f_{\rm tr} \tag{12}$$

where $\Delta f_{\rm b} \equiv (\Delta f_{\rm T} + \Delta f_{\rm v})$ is the sum of the thermal and viscous boundary layer perturbations, respectively; $\Delta f_{\rm d}$ is the perturbation from a fill duct; $\Delta f_{\rm sh} \equiv \Delta f_{\rm sh1} + \Delta f_{\rm sh2} + \Delta f_{\rm sh3} + \Delta f_{\rm sh4}$ is the sum of the perturbations from the shell's motion, and $\Delta f_{\rm tr}$ is the perturbation from the transducers.

The relation,

$$k_{\rm B} = \lim_{p\to 0}\frac{mc^2}{\gamma T_{\rm TPW}} = \frac{m}{\gamma T_{\rm TPW}}\left(\frac{2L}{l}\right)^2 \lim_{p\to 0}\left(f_N - \Delta f_{\rm b} - \Delta f_{\rm d} - \Delta f_{\rm sh} - \Delta f_{\rm tr}\right)^2 \tag{13}$$

connects the measured resonance frequency f_N to the various frequency perturbations and to the Boltzmann constant. (Here, $T_{\rm TPW}$ denotes the temperature of the triple point of water and m is the average atomic mass of the gas.) If the frequency perturbations in Eq. 13 are mutually independent, the terms $2u\,(\Delta f_{\rm b})/f_{\rm R}$, $2u\,(\Delta f_{\rm d})/f_{\rm R}$, $2u\,(\Delta f_{\rm sh})/f_{\rm R}$, and $2u\,(\Delta f_{\rm tr})/f_{\rm R}$ must be added in quadrature to other contributions to the relative standard uncertainty of the Boltzmann constant, $u_{\rm r}(k_{\rm B})$. First, we consider the thermo-acoustic boundary perturbation $\Delta f_{\rm b}$ and then we consider the sum of the perturbations from the shell's motion $\Delta f_{\rm sh}$. Although $\Delta f_{\rm b} > \Delta f_{\rm sh}$, we shall conclude that the relative uncertainties obey the opposite inequality $u_{\rm r}(\Delta f_{\rm b}) < u_{\rm r}(\Delta f_{\rm sh})$.

In reference [20], one of us (MRM) estimated the relative uncertainties of the viscosity $u_{\rm r}(\eta_{\rm Ar}) \approx 0.00025$ and the thermal conductivity $u_{\rm r}(\lambda_{\rm Ar}) \approx 0.00025$ of

argon in the limit of zero density at 273.16 K. Using these estimates in Eqs. 4 and 5 leads to an estimated relative uncertainty of the thermo-acoustic boundary layer correction: $u_r(\Delta f_b) \approx 0.00013$. For the worst case in Table 1, ($L = 80.7\,\text{mm}, l = 1, p = 100\,\text{kPa}$), $\Delta f_b/f^0 \approx \Delta f_b/f_R \approx -0.0015$ and its contribution to $u_r(k_B)$ is $2u(\Delta f_b)/f_R \approx 4 \times 10^{-7}$. This contribution is so small that other contributions to $u_r(k_B)$ will dominate the uncertainty budget. However, a skeptical metrologist might argue that this contribution to $u_r(k_B)$ is an underestimate for two reasons. First, the values of $u_r(\eta_{Ar})$ and $u_r(\lambda_{Ar})$ rely on the work of only one group [21] that measured the ratio $(\eta_{argon})/(\eta_{helium})$ with the extraordinarily small claimed uncertainty of 0.00011. Second, the calculation of boundary perturbation Δf_b via Eqs. 4 and 5 is correct only to the first order in the small quantities, δ_T/a and δ_v/a. A calculation that includes the terms $(\delta_T/a)^2$ and $(\delta_v/a)^2$ is needed for additional confidence. These concerns lead us to discuss in Sect. 6, a method of partially canceling this comparatively large contribution to $u_r(k_B)$.

Among the model shell motions considered for Table 1, the largest perturbation for $l = \{\text{even}\}$ is $\Delta f_{sh3}/f^0$ which resulted from the bending of the endplates. When the gas is at 100 kPa, this perturbation ranges from -20.2×10^{-6} to 11.9×10^{-6}. As mentioned above, these values were calculated by assuming that the position of each endplate was pinned to the end of the cylinder, but free to bend. If a clamped boundary condition is assumed, the calculated perturbations are reduced by about a factor of 10. This end-plate bending perturbation and the other perturbations from the shell's mechanical admittance are linear functions of the gas pressure that vanish at zero pressure. Thus, these perturbations will not contribute to k_B if they are not too large and if the resonance frequencies are linearly extrapolated to zero pressure. A rare exception to the linear pressure dependence occurs when a resonance frequency of the shell's motion is near the resonance frequency of a gas mode. Such gas modes should not be used for measuring k_B.

The frequency shifts and half-width contributions for the shell's motion depend upon the medium surrounding the resonator and the structure supporting the resonator. When the surrounding medium is a gas, the energy radiated is negligible because of the large mismatch of the acoustic impedances of the gas and the heavy-walled shell. The exchange of momentum and energy between the shell and its supports can be reduced by making the supports weak, where "weak" means that the resonance frequencies of the shell moving with respect to its supports are well below the gas resonance frequencies f^0_{lmn}.

For completeness, we mention two smaller perturbations. First, the attenuation of sound throughout the volume of the cavity reduces the resonance frequencies and increases the half-widths by terms of order $\omega D_v/c^2 \sim \omega D_T/c^2 \sim (l\delta_T/L)^2$. These terms can be calculated accurately from the formulas in Ref. [22] and the properties of the gas. Second, there are perturbations to the frequencies from the thermal and momentum accommodation coefficients [23]. These perturbations cannot be predicted because they depend upon the gas–metal interactions on the scale of atomic sizes. Instead, these perturbations must be determined by including a p^{-1} term when fitting frequency-vs.-pressure data on an isotherm. In Sect. 6, we show that the effects of imperfect thermal accommodation on the endplates of the cavities can be canceled using two cylindrical cavities.

4 Measurement of Resonance Frequency

4.1 Overview of Apparatus

The gas supplied to the resonator's cavity is independent of the gas supplied to the pressure vessel. The pressure in the cavity is the sum of the pressure in the pressure vessel and the pressure indicated by the differential pressure gauge between the cavity and the pressure in the pressure vessel. This arrangement minimizes the chance of contaminating the gas in the cavity.

Each cylindrical resonator has two fused-silica endplates that admit laser beams into and out of the cavity. The inside-facing surface of each endplate was coated with a partially reflecting metal film. The walls of the cavity were bearing-steel cylinders with ends ground flat to 0.3 μm. The ends of the cylinder were specified to be parallel within 0.5 μm across the diameter. A CCD video recorder and related optical components were built inside the pressure vessel to record the optical interference patterns in situ.

The resonator was supported with its cylindrical axis vertical on a moveable stage. The stage could translate the resonator horizontally and rotate it about the cylindrical axis.

4.2 Frequency Measurement

We used the same procedure described in the literature [24] for fixed-path gas resonators to measure the resonance frequencies f_N and the half-widths g_N of the cylindrical cavity. First, the resonance frequency f_N and the half-width g_N were estimated from either a preliminary measurement or from a theoretical model. Then, the drive transducer was stepped in increments of $g_N/5$ through 11 synthesized, discrete frequencies starting at $f_N - g_N$ and ending at $f_N + g_N$. Then, the frequency sweep was reversed by starting at $f_N + g_N$ and ending at $f_N - g_N$. At each frequency, the in-phase voltage u and the quadrature voltage v generated by the detector transducer were measured by a lock-in amplifier. The 11 frequencies and 44 voltages were fitted by the resonance function:

$$u + \mathrm{i}v = \frac{\mathrm{i}fA}{f^2 - (f_N + \mathrm{i}g_N)^2} + B + C(f - \tilde{f}) \tag{14}$$

Here, A, B, and C are complex constants; $F_N = f_N + \mathrm{i}g_N$ is the complex resonance frequency of the mode under study; and the parameter $\tilde{f}$ is fixed and is usually taken as the average frequency for the data in the fit. The parameters B and C account for the effects of possible crosstalk and the "tails" of the modes other than f_N.

We conducted simple experiments to compare 6 mm diameter capacitor microphone cartridges with 6 mm diameter PZT transducers. For the comparison, we used a prototype cylindrical resonator, 80.7 mm long and 80 mm in diameter, in ambient air without temperature controls. First, we used one of the capacitor microphones to generate sound and the other to detect sound, as described in the literature [6,8,9,12]. The measurement procedure described in the preceding paragraph resulted in the values

$f_N = 2124.24\,\text{Hz}$ and $g_N = 2.1$ for the (1,0,0) longitudinal mode. The resonance function was fitted with a relative standard deviation of 1.5×10^{-3}, which corresponds to determining the perturbed resonance frequency f_R with the uncertainty $u_r(f_R) = 1.5 \times 10^{-6}$.

Next, we replaced the endplates containing the microphones with all-metal endplates designed to test the PZT transducers. Each of these endplates had a blind hole that had been machined into the outside-facing surface to form a diaphragm flush with the inside surface, thereby preserving the cylindrical shape of the cavity. The diaphragm had a diameter of 10 mm and a thickness of 0.3 mm. A PZT transducer (6.4 mm diameter and 0.4 mm thick) was cemented to the outside surface of each diaphragm with epoxy. The location of the drive and the detector PZTs on opposite endplates minimized electrical crosstalk between them. The drive PZT was excited with 7 V (root mean square), and it dissipated 1.0 μW at 2121 Hz. Under these conditions, the standard deviation of the voltages from a fit by Eq. 14 was 2.0×10^{-4}, a factor of 7 smaller than we obtained with the capacitor microphones. As a result, the perturbed resonance frequency was determined with a fractional uncertainty of 2.0×10^{-7}.

We tested diaphragms with thicknesses t_{dm} of 0.3 mm, 0.4 mm, and 0.5 mm. Our simple model predicts that the signal-to-noise ratio varies as $1/t_{dm}^3$ for each diaphragm, or $1/t_{dm}^6$ for the source and detector together. Consistent with this prediction, Fig. 2 shows that the detected signal decreased by a factor of approximately 20 when the thickness of both diaphragms was increased from 0.3 mm to 0.5 mm.

When fitting Eq. 14 to data, the resonance half-width g_R is usually treated as a frequency-independent parameter. In reality, the contributions to the resonance half-width include the terms g_v in Eq. 4 and g_T in Eq. 5 that vary as $f^{-1/2}$. To account for these terms, we follow Gillis et al. [22] and replace g_N in Eq. 14 with $g_N(f_N/f)^{1/2}$. The resulting resonance function is no longer symmetrical about f_N, and the best-fit values of f_N and g_N must be corrected using

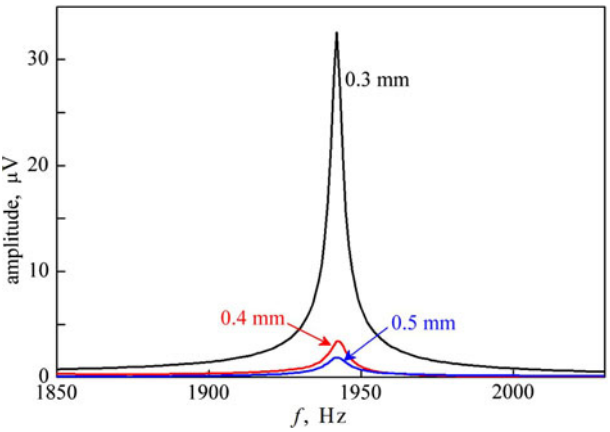

Fig. 2 Frequency scan through (1,0,0) mode using diaphragms of various thicknesses

$$f_{\text{corrected}} - f_N = -f_N/(8Q^2) \quad \text{and} \quad g_{\text{corrected}} - g_N = -g_N/(4Q^2). \tag{15}$$

(This correction accounts only for the frequency-dependence of the thermo-acoustic boundary layer.) During the 1988 re-determination of k_B [12], this correction was small enough to be ignored because $Q \geq 1375$; however, in this work the fractional correction to the frequency becomes as large as 10^{-6} and the fractional correction to k_B becomes as large as 2×10^{-6}.

We also investigated the effect of adding the term $D(f - \tilde{f})^2$ to the right-hand side of Eq. 14. This term changed the best-fit values of f_N by -0.002 Hz for each of the modes $(1, 0, 0), \ldots, (5, 0, 0)$. The -0.002 Hz change corresponds to fractional frequency changes ranging from -1×10^{-6} to -0.2×10^{-6} and will be investigated in future work.

In order to accurately measure the frequencies of the non-degenerate $(l, 0, 0)$ modes, they must be well separated from the frequencies of the other modes of the cylindrical cavity. For modes of comparable amplitude, "well separated" means a separation on the order of three times the sum of the half-width of the $(l, 0, 0)$ mode and the half-width of any nearby, interfering mode. Perhaps, this criterion can be relaxed if the amplitude of the interfering mode is much smaller than the amplitude of the $(l, 0, 0)$ mode. The possibility of altering the relative amplitudes of the modes led us to explore the effects of locating one of the transducers at a distance d off the symmetry axis. For example, if the transmitting transducer is placed at $d/a = 0.618$, its center will lie on the node of the first radial mode. In this situation, in a first approximation, the transmitter will not excite any of the modes with indices $(l, m, 1)$. As shown in Fig. 3, the theory does indeed apply to our prototype cavity. Specifically, when one transducer was located at $d/a = 0.618$ (off the symmetry axis), the amplitudes of the

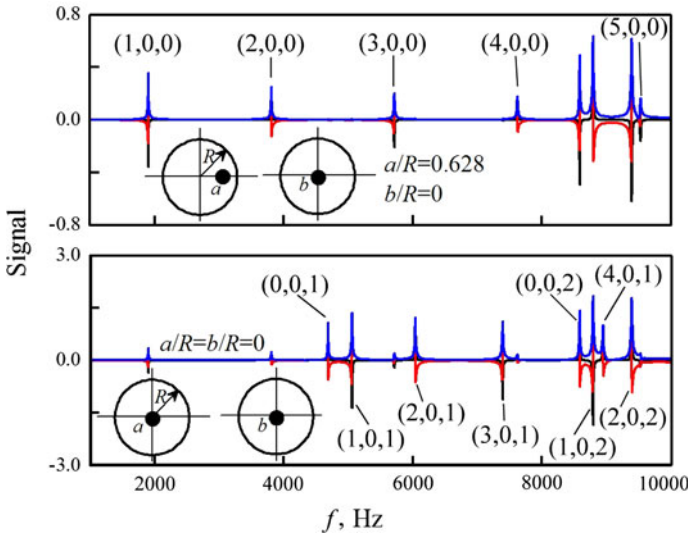

Fig. 3 Effect of transducer location on the relative amplitudes of the $(l, 0, 0)$ and $(l, m, 1)$ modes at 293 K and 100 kPa in argon

(0, 0, 1), (1, 0, 1), (2, 0, 1), (3, 0, 1), and (4, 0, 1) modes were reduced in comparison with the amplitudes of the (l, 0, 0) modes. With confidence, we conclude that d/a can be chosen for each transducer to suppress any single mode that has a node on the endplates.

5 Length Measurements

We used two-color interferometry to determine the length of each cylindrical cavity in situ. Figure 4 sketches the principle of the measurement. The two-color setup consisted of a stabilized He–Ne laser (nominal wavelength 633 nm) and a semiconductor laser (nominal wavelength 657 nm). A wavelength meter was installed for in situ calibration of the semiconductor laser relative to the He–Ne laser. The frequency stability of the semiconductor laser was better than 5×10^{-7}.

The endplates of the resonator were made of optical-quality quartz glass. The inside surface of each endplate was coated with a metallic film to increase its reflectivity. When the endplates were bolted to the cylinder, a small angle existed between the metallic films. The two laser beams entered the cavity perpendicular to one film forming two different equal-inclination interference patterns. The analysis of the fringe patterns is discussed in Ref. [25].

The laser beams penetrate into the partially reflecting films on the order of 20 nm [26,27]. Thus, the optical length of each cylindrical cavity L_{opt} determined by two-color interferometry will have an unknown bias on the order of 40 nm. However, this bias will cancel out from the difference between the optical lengths of two cavities provided that the same endplates are used on both the cavities. We plan to exploit this cancellation by using a two-cylinder procedure to measure the speed of sound.

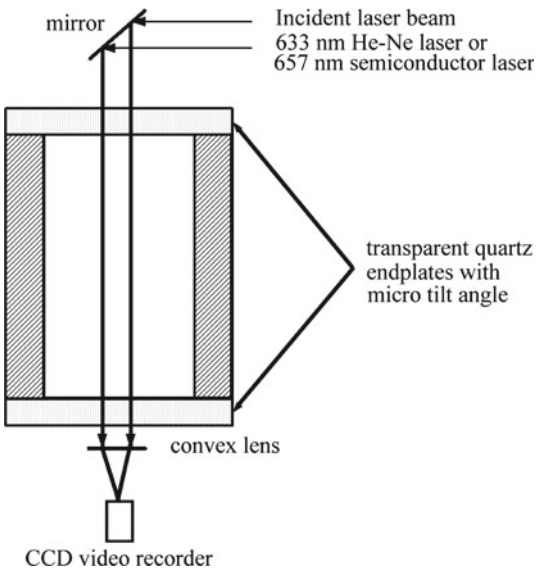

Fig. 4 Sketch of two-color interferometer

6 Two-Cylinder Method

The fundamental assumption of the two-cylinder method is: the difference between the optical lengths ($L_{\text{opt}-1} - L_{\text{opt}-2}$) of two cavities is identical to the difference between the acoustic lengths ($L_1 - L_2$) of the same two cavities. Thus, we use the relation,

$$\Delta L_{12} = L_1 - L_2 = L_{\text{opt}-1} - L_{\text{opt}-2} = \frac{c}{2}\left(\frac{l_1}{f_1^0} - \frac{l_2}{f_2^0}\right) = \frac{c}{2}\left(\frac{l_1}{f_1} - \frac{l_2}{f_2}\right) + \delta L_{12}, \tag{16}$$

where the subscripts 1 and 2 refer to the 1st and 2nd cylinders, and δL_{12} is a small correction due to the perturbations discussed in Sect. 3. The parameters l_j, f_j, and f_j^0 refer to the longitudinal mode index, the measured resonance frequency, and the corresponding unperturbed frequency, respectively, of the longitudinal mode studied in cylinder j. Now, we show that particular choices of l_1, l_2, L_1, and L_2 are useful for reducing the effects of particular perturbations.

6.1 Reducing the Effects of the Thermoacoustic Boundary Layer

The working equation for the speed of sound is derived from Eq. 16,

$$c = \frac{2 f_1 f_2 \Delta L_{12}}{l_1 f_2 - l_2 f_1}\left(1 - \frac{\delta L_{12}}{\Delta L_{12}}\right) \tag{17}$$

where the small correction $\delta L_{12}/\Delta L_{12}$ is, to lowest order,

$$\frac{\delta L_{12}}{\Delta L_{12}} = \frac{1}{\Delta L_{12}}\left(L_1 \frac{\Delta f_1}{f_1^0} - L_2 \frac{\Delta f_2}{f_2^0}\right) + \mathrm{O}\left[(\Delta f/f)^2\right]. \tag{18}$$

The frequency shifts Δf_1 and Δf_2 denote the sum of perturbations of the boundary layer, the gas fill duct, the transducers, and the shell motion in the two resonators at the same temperature and pressure. Since the correction in Eq. 18 depends on the difference of terms, we looked for conditions for which the difference, and hence the correction, is small. We investigated the dependence of Eq. 18 on the length ratio of the two cylinders and on the mode–index ratio of the longitudinal modes studied. We define $b \equiv L_1/L_2$, with $b > 1$, and $s \equiv l_1/l_2$, so that $f_1^0 = f_2^0 s/b$ and $\Delta L_{12} = L_2(b-1)$. We substitute these relations into Eq. 18 to obtain

$$\frac{\delta L_{12}}{\Delta L_{12}} = \frac{1}{f_2^0}\frac{1}{b-1}\left(\frac{b^2}{s}\Delta f_1 - \Delta f_2\right). \tag{19}$$

The frequency shifts Δf_1 and Δf_2 are functions of b, s, L_2, l_2, T, and p.

Table 2 Length correction and its uncertainty for the two-cylinder method with $L_2 = 80.7$ mm at 273.16 K and $p = 100$ kPa

b	s	Mode		$\delta L_{12}/\Delta L_{12}$ ($\times 10^6$)	$u(\delta L_{12})/\Delta L_{12}$ ($\times 10^6$)
		l_2	l_1		
1.6	2	2	4	−464	24[a]
1.6	2	4	8	−352	58[a]
1.6	3	2	6	−68	30[a]
1.6	3	4	12	−46	48[a]
2.0	2	2	4	−720	3.2[b]
2.0	2	4	8	−510	3.2[b]

[a] The uncertainty at 100 kPa is dominated by endplate bending; however, this contribution will extrapolate to zero as $p \to 0$

[b] The uncertainty at 100 kPa is dominated by radial and axial stretching which should extrapolate to zero as $p \to 0$

In this study, we chose the lengths of the resonators to have the ratio $b = 1.6$ ($L_1 = 129.14$ mm and $L_2 = 80.7$ mm) because this choice resulted in significant cancellation of the boundary layer perturbation, the largest perturbations in Table 1. The estimates of the correction given by Eq. 19 for resonators filled with argon at 273.16 K and 100 kPa are given in Table 2. We recall that the free body recoil does not generate a perturbation for even modes. Therefore, the preferred modes are those with $l_1 = 6, 12$ and $l_2 = 2, 4$ for $s = 3$, and $l_1 = 4, 8, 12$ and $l_2 = 2, 4, 6$ for $s = 2$.

The total uncertainty in δL_{12} is included in Table 2. The perturbations generated by the boundary layers and the fill duct can be modeled with sufficient accuracy to correct the measurements. The accuracy of the boundary layer perturbation correction is limited by the thermal conductivity of gas. For argon, the thermal conductivity is known with an uncertainty of 0.025 % (Sect. 3.2). Therefore, we can correct the resonance frequencies for the boundary layer perturbations in a single resonator with an uncertainty of 0.13×10^{-6}. Using two resonators that are tuned to reduce the boundary layer perturbations ($b = 1.6, s = 3$), the uncertainty in the frequency correction for the boundary layer is reduced to 0.02×10^{-6}. In hindsight, this method of tuning the resonators' dimensions and the mode ratios to cancel the boundary layer perturbation does not reduce the uncertainty in the determination of k_B, because the boundary layer correction can be calculated with very high accuracy, whereas the correction from the shell motion has a much higher uncertainty. In particular, for $b = 1.6$, the uncertainty is dominated by the large uncertainty in $\Delta f_{sh3}/f^0$ due to endplate bending.

The last entry for $b = 1.6$ in Table 2 assumes that the resonance frequency of the (12, 0, 0) mode $f_{12,0,0}$ will be accurately measured for a cavity with $L_1 = 129.14$ mm and $2a = 80$ mm. In practice, this may be impossible because many other modes have nearly the same frequency, as shown in Table 3. Table 3 lists the mode indices, the dimensionless wave-vector $ka \equiv 2\pi f a/c$, and the half-width of each mode expressed as a wave-vector difference: $\Delta ka \equiv 2\pi g a/c$. Although five values of ka are listed near $f_{12,0,0}$, there are nine modes in this frequency interval because the modes with $m \neq 0$ are doubly degenerate. Any two of these nearby modes can be suppressed by

Table 3 Wave-vectors and half-widths of the acoustic modes of a cylindrical cavity with $L = 129.14$ mm and $2a = 80$ mm near the (12, 0, 0) mode

The calculation of Δka assumes that the cavity is filled with argon at 100 kPa and 273.16 K

Mode indices	ka	Δka
(10, 5, 0)	11.655	0.024
(12, 0, 0)	11.677	0.011
(0, 1, 3)	11.706	0.006
(3, 3, 2)	11.715	0.010
(6, 0, 3)	11.730	0.010
(0, 6, 1)	11.735	0.010

locating the two transducers on nodes of these modes. Nevertheless, we conclude that it will be difficult to measure $f_{12,0,0}$ accurately.

6.2 Reducing the Effect of the Endplates

In Sect. 3.1.2, we noted that the perturbation from the bending of the endplates cannot be calculated accurately because the elastic boundary condition where the quartz endplates join the sides of the metal cylinders is not accurately known. Furthermore, the boundary condition might change every time the joint is disassembled and reassembled.

The effects of endplate bending can be eliminated almost entirely by using two cylinders with lengths in a 2:1 ratio (i.e., $L_2 = 2L_1$) and using modes in a 2:1 ratio (i.e., $l_2 = 2l_1$) as shown in the last two rows of Table 2. With these choices, the two cavities operate at nearly the same frequencies; therefore, the frequency-dependent admittances of the cavities' endplates will be nearly identical for both the cavities. Thus, the effects of endplate bending as well as the effects of a fill duct located in one end and the thermal admittance of the ends (including the effect of imperfect thermal accommodation) will be nearly identical for both the cavities and will cancel out for the determination of the speed of sound and k_B.

It is possible to avoid disassembly and reassembly of the fragile joints between the quartz endplates and the steel cylinder by assembling the two cavities from three subassemblies such as those sketched in Fig. 5. Although we have not tested this concept yet, the flanged joints between sections of a steel cylinder can be robust, and, we expect, assembled reproducibly. Concerning reproducibility, we cite on an international comparison which required wringing together pairs of steel gauge blocks [28]. The standard deviation of the repeatability of the lengths of assembled pairs of blocks ranged from 3 nm to 12 nm, depending on the laboratory.

A joint between two sections of the resonator will perturb the resonance frequencies if it is located at a pressure anti-node and if the width of the gap between the sections is comparable to the boundary layer thickness. The joints at the endplates are always located at pressure anti-nodes. When the resonator in Fig. 5 is assembled without the center section, the joint between the sections will lie at a pressure anti-node for all even-numbered modes ($l_1 = 2, 4, \ldots$). When the center section is used, the joints, located 1/4 of the resonator length from each endplate, will lie at pressure anti-nodes

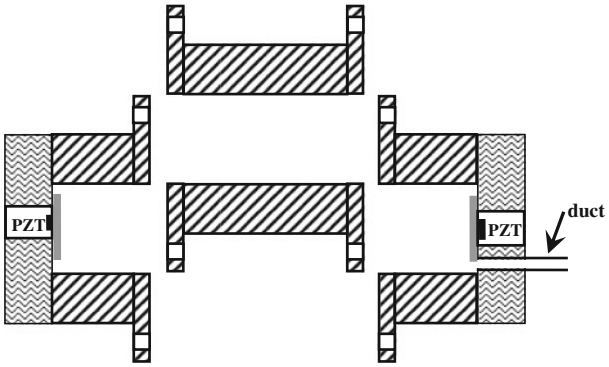

Fig. 5 Conceptual design of three components that form two cylindrical resonators designed to cancel perturbations from endplates. In one configuration, both ends constitute a resonator. In the second configuration, the middle section is inserted between the ends to double the length of the resonator

for $l_2 = 2l_1 = 4, 8, \ldots$ (twice the even-numbered modes of the shorter resonator). We conclude that the surfaces of all the joints should be lapped to minimize the gaps. The joints at the endplates need not be disassembled, so those gaps may be permanently filled.

7 Projected Uncertainty Budget

We use Eq. 17 as a starting point for the discussion of a projected uncertainty budget for re-determining k_B using the two-cylinder method for measuring the speed of sound in argon. For argon, the zero-pressure heat capacity ratio γ_0 is exactly 5/3. We expect to control and measure the temperature of the working gas near T_{TPW} with an uncertainty of 0.2 mK, which contributes the relative uncertainty $u_r(T) = 0.73 \times 10^{-6}$ to the determination of k_B. The Avogadro constant has a relative uncertainty $u_r(A) = 0.5 \times 10^{-8}$ [29]. The noble gas impurities in the argon and the uncertain relative isotope abundances contribute to the uncertainty of the molecular weight M. The previous work of Moldover et al. [12] attained the uncertainty $u_r(M) = 0.7 \times 10^{-6}$; we expect to equal this. The speed of sound is obtained from the difference between the lengths of the two cylindrical resonators ΔL_{12} and the resonant frequency of a non-degenerate longitudinal mode. From Sect. 5, we expect to achieve $u_r(L_1) = u_r(L_2) = 5 \times 10^{-7}$ and therefore $u_r(\Delta L_{12}) = 7 \times 10^{-7}$. As indicated in Sect. 4, the relative uncertainty of measuring the (1, 0, 0) resonance frequency at 100 kPa was $u_r(f_{1,0,0}) = 2.0 \times 10^{-7}$, assuming we use 0.3 mm diaphragms. This uncertainty will be smaller at higher pressures and for the modes $(l, 0, 0)$ with $l > 1$. However, this uncertainty does not propagate in a simple way into a component of $u_r(k_B)$. We now discuss this propagation.

As in previous acoustic determinations of k_B, the resonance frequencies of each resonator measured on the isotherm T_{TPW} can be corrected for the well-known, gas-dependent, perturbations (e.g., thermo-acoustic boundary layer). Then, the corrected frequencies and lengths from the two cylinders are combined and fitted by the polynomial function,

$$c = \frac{2 f_1 f_2 \Delta L_{12}}{l_1 f_2 - l_2 f_1} \left(1 - \frac{\delta L_{12}}{\Delta L_{12}}\right) = \sum_{i=-1}^{3} A_i p^i, \tag{20}$$

where A_1, A_2, and A_3 are the acoustic virial coefficients, A_{-1} accounts for thermal and viscous accommodation coefficients, and $A_0 = N_A k_B T_{TPW} \gamma_0 / M$. Thus, the uncertainty of k_B will have contributions from the correlations among the parameters in Eq. 20 that are much larger than $u_r(f_{lmn})$. These correlations will depend upon the range of the fitted data. We have not completed an analysis appropriate to the two-cylinder method; therefore, we now outline the complications and conclude by guessing the uncertainty contribution from fitting the data.

First, we recall, that in the context of re-determining k_B using argon in a quasi-spherical cavity resonator, one of us (MRM) observed that the lowest uncertainties can be obtained by measuring acoustic resonance frequencies in the range from 100 kPa to 500 kPa [20]. At still lower pressures, the perturbations from the thermo-acoustic boundary layer and the accommodation coefficients diverge; at higher pressures, the perturbations from the elastic response of the shell become excessive. The same considerations apply to the two-cylinder method, and approximately the same pressure range is optimum. (Note: A cylinder is less rigid than a quasi-sphere if both are made of the same material and both have the same ratio $\Re = \{\text{shell thickness}\}/\{\text{radius}\}$. Therefore, we made our prototype cylinders with $\Re \approx 0.6$ which is significantly larger than the value $\Re \approx 0.2$ that has been used for spherical and quasi-spherical acoustic thermometers [6,8,9].) Second, the parameter A_3, in Eq. 20 will be taken from the literature of speed-of-sound measurements at high pressures without adding significant uncertainties. Third, the parameter A_1 will be frequency-dependent, hence mode-dependent, because it accounts for the linear pressure dependence of the various shell perturbations as well as the linear pressure dependence of the speed of sound in argon.

With the above complications in mind, we recall that the 1988 re-determination of k_B relied on frequency measurements with a relative uncertainty that was 0.5 times the relative uncertainty we have demonstrated here under comparable conditions. We can offset this factor of 0.5 using the present, fully automated, apparatus to acquire 5 to 10 times the amount of data that was acquired in 1988. Thus, we expect to achieve approximately the same relative uncertainty $u_r(A_0) \sim 0.7 \times 10^{-6}$ that was achieved in 1988. In Table 4, we summarize the uncertainty estimates that lead to the projected uncertainty $u_r(k_B) = 1.5 \times 10^{-6}$.

Table 4 Projected uncertainty budget for re-determining the Boltzmann constant by the two-cylinder method

Uncertainty source	Uncertainty ($\times 10^6$)
Gas temperature measurement	0.73
Avogadro constant	0.10
Molecular weight determination	0.70
Cylinder length difference	0.70
Fitting A_0 to frequency measurements[a]	0.70
Combined uncertainty	1.47

[a] Assumes 0.3 mm thick diaphragms are used

8 Summary and Discussion

We report significant progress in developing the two-cylinder method of measuring the Boltzmann constant. We are able to account for the comparatively low Qs of the $(l, 0, 0)$ modes using an asymmetric resonance function. We improved the signal-to-noise ratio of the frequency measurements by a factor of 8 by replacing capacitive electro-acoustic transducers with piezoelectric transducers. By selecting the ratio of the cavity lengths and by choosing the modes to study, we can reduce either the perturbations from the endplates or the perturbations from the thermo-acoustic boundary layer. The perturbed resonance frequency is determined for this mode of the resonance frequency. By locating the transducer diaphragms on a node, we can suppress a particular mode that is close to the modes $(l, 0, 0)$ chosen for measurement.

We adapted the two-color laser interference method for determining the lengths of gauge blocks to determining the interior length of an acoustic cavity at ambient temperature. We will use the two-color laser interferometer in its single wavelength mode as a dilatometer to measure the thermal contraction of the length in situ. In summary, the current investigation demonstrates that the two-cylinder method for determining k_B is likely to achieve an uncertainty that is comparable to the uncertainty of spherical resonators.

The present acoustic method of re-determining k_B relies on an optical measurement of the change in the length of a cavity. This differs significantly from the presently accepted determination of k_B [12] that relied on measuring the volume of a spherical cavity by weighing the mercury required to fill the cavity.

Acknowledgments The authors would like to thank D. Ripple and F. Pavese for their helpful suggestions to prevent gas contamination. This work was supported by the National Science and Technology Pillar Program (2006BAF06B00) and the National Natural Science Foundation of China (No. 50906076).

References

1. K.A. Gillis, M.R. Moldover, Int. J. Thermophys. **17**, 1305 (1996)
2. J.J. Hurly, K.A. Gillis, J.B. Mehl, M.R. Moldover, Int. J. Thermophys. **24**, 1441 (2003)
3. K.A. Gillis, Int. J. Thermophys. **15**, 821 (1994)
4. J.F. Estela-Uribe, J.P.M. Trusler, Int. J. Thermophys. **21**, 1033 (2000)
5. J.P.M. Trusler, Int. J. Thermophys. **18**, 635 (1997)
6. M.R. Moldover, S.J. Boyes, C.W. Meyer, A.R.H. Goodwin, J. Res. Natl. Inst. Stand. Technol. **104**, 11 (1999)
7. M.B. Ewing, J.P.M. Trusler, J. Chem. Thermodyn. **32**, 1229 (2000)
8. G. Benedetto, R.M. Gavioso, R. Spagnolo, P. Marcarino, A. Merlone, Metrologia **41**, 74 (2004)
9. L. Pitre, M. Moldover, W.L. Tew, Metrologia **43**, 142 (2006)
10. D.C. Ripple, G.F. Strouse, M.R. Moldover, Int. J. Thermophys. **28**, 1789 (2007)
11. A.R. Colclough, T.J. Quinn, T.R.D. Chandler, Proc. R. Soc. Lond. A **368**, 125 (1979)
12. M.R. Moldover, J.P.M. Trusler, T.J. Edwards, J.B. Mehl, R.S. Davis, J. Res. Natl. Bur. Stand. **93**, 85 (1988)
13. J. Fischer, S. Gerasimov, K.D. Hill, G. Machin, M. Moldover, L. Pitre, P. Steur, M. Stock, O. Tamura, H. Ugar, R. White, I. Yang, J. Zhang, Int. J. Thermophys. **28**, 1753 (2007)
14. T.J. Quinn, A.R. Colclough, T.R.D. Chandler, Phil. Trans. R. Soc. Lond. A **283**, 367 (1976)
15. P.M. Morse, K.U. Ingard, *Theoretical Acoustics*, vol. 606 (McGraw-Hill Book Co, New York, 1968), pp. 554–557

16. J.P.M. Trusler, *Physical Acoustics and Metrology of Fluids* (Adam Hilger, IOP Publishing Ltd, Bristol, 1991)
17. M.C. Junger, D. Feit, *Sound, Structures, and Their Interaction* (MIT Press, Cambridge, 1986), pp. 195–234
18. H. Lin, K.A. Gillis, J.T. Zhang, Int. J. Thermophys. (in press, 2010)
19. K.A. Gillis, H. Lin, M.R. Moldover, J. Res. Natl. Inst. Stand. Technol. **114**, 263 (2009)
20. M.R. Moldover, C.R. Phys. **10**, 815 (2009)
21. E.F. May, M.R. Moldover, R.F. Berg, Int. J. Thermophys. **28**, 1085 (2007)
22. K.A. Gillis, I.I. Shinder, M.R. Moldover, Phys. Rev. E **70**, 021201 (2004)
23. J.P.M. Trusler, *Physical Acoustics and Metrology of Fluids* (Adam Hilger, IOP Publishing Ltd, Bristol, 1991), pp. 44–47
24. M.R. Moldover, J.B. Mehl, M. Greenspan, J. Acoust. Soc. Am. **79**, 253 (1986)
25. C.R. Tilford, Appl. Opt. **16**, 1857 (1977)
26. E.D. Palik (ed.), *Handbook of Optical Constants of Solids* (Academic Press New York 1985), pp. 275–804
27. N. Barakat, S. Mokhtar, K.A. el Haadi, J. Opt. Soc. Am. **54**, 213 (1964)
28. R. Thalmann, Metrologia **39**, 165 (2002)
29. P.J. Mohr, B.N. Taylor, D.B. Newell, Rev. Mod. Phys. **80**, 633 (2008)